Wind-tunnel experiments on atmospheric heavy gas dispersion: Metrological aspects

Cristina Vidali, Massimo Marro, Horacio Correia, Louis Gostiaux, Simon Jallais, Deborah Houssin, Elena Vyazmina, Pietro Salizzoni

Wind-tunnel experiments on atmospheric heavy gas dispersion: metrological aspects

Cristina Vidali[a,b,*], Massimo Marro[a], Horacio Correia[a], Louis Gostiaux[a], Simon Jallais[b], Deborah Houssin[b], Elena Vyazmina[b], Pietro Salizzoni[a]

[a] *Univ Lyon, Ecole Centrale de Lyon, CNRS, Univ Claude Bernard Lyon 1, INSA Lyon, LMFA, UMR5509, 69130, Ecully, France*
[b] *Air Liquide Paris Research & Development Center, Paris Innovation Campus, 1 chemin de la Porte des Loges, Les Loges-en-Josas, Jouy-en-Josas, France.*

Abstract

We propose a new experimental protocol to investigate the atmospheric dispersion of a dense gas in wind-tunnel experiments. Simultaneous measurements of concentration and velocity are performed by coupling a flame ionization detector (FID) and a hot-wire anemometer (HWA), whose probes are located sufficiently close to each other so that the respective measurements correspond to a same sampling volume. The heavy gas emission consists in a mixture of air, carbon dioxide, and ethane. Carbon dioxide is used as a buoyant agent, and ethane is used as a tracer, its concentration being detected by the FID. In this context, the main metrological issue of the setup concerns the response of the FID and the HWA to different proportions of the two gases in the mixture. Notably, the presence of carbon dioxide affects the linear response of the FID, which can attain a saturation level, as well as the response of the HWA, due to the varying density of the gas. This can be compensated by determining a non-linear calibration curve of the FID, which is used to determine the instantaneous fluid density, and to apply a time-dependent correction to the HWA response. To analyse the performances of the coupled HWA-FID system we realised wind-tunnel experiments of tracer dispersion in a turbulent boundary layer. The estimate of mass fluxes through different sections downwind the source enlightens the reliability of the experimental results, and show that the measurements within a negatively buoyant gas plume are as

*Corresponding author
Email address: cristina.vidali@ec-lyon.fr (Cristina Vidali)

accurate as those within a passive scalar plume.

Keywords: Calibration, hot-wire anemometry, flame ionization detector, wind tunnel, heavy gas dispersion

1. Introduction

Experimental studies in atmospheric wind tunnels still play a major role for our understanding of the physics of pollutant dispersion. Furthermore, these studies provide reference datasets, that can be subsequently used to validate and improve numerical models. The large majority of the experiments performed so far concerned the case of passive (neutrally buoyant) releases, but relatively few studies focused on the case of buoyant gases. Therefore, there is a clear need to improve the characterisation of turbulent fluctuations and mass fluxes within dense gas plumes [1], which requires combined statistics of instantaneous concentration and velocity.

The experimental investigation of the turbulent dispersion of buoyant releases can be performed in both wind tunnels and water flumes. However, the latter are not suited for the simulation of releases characterised by large density differences with the ambient fluid. Indeed, as enlightened by Meroney [2], experiments using salt as a density ingredient can be hardly performed with density differences exceeding 10%. We will therefore focus here only on wind-tunnel experiments, in which gases with molecular weight higher than that of air are employed for the simulation of heavy gas releases.

Combined statistics of concentration and velocity can be actually acquired adopting suitable measurement techniques. Different systems have been developed and employed in wind-tunnel experiments, involving techniques for the measurements of velocity as the hot-wire anemometry (HWA) and the laser Doppler anemometry (LDA). Measurements of scalar concentrations include instead the photo ionization detector (PID), the cold film/wire, and the flame ionization detector (FID).

The HWA [3] is a well established technique, widely employed to measure fluctuating fluid velocities. The calibration procedure is well defined in isodensity flows, but is more complicated for gases with varying density [4, 5, 6, 7, 8]. In order to measure the velocity in gas mixtures (in isothermal conditions), Corrsin [9] combined the cali-

brations of HWA obtained for each gas. However, this method led to systematic errors in the estimate of the coefficients of the calibration King's equation. Pitts and McCaffrey [6] calibrated the hot-wire and film anemometers in different gases and defined an empirical correction of the calibration parameters as a function of the Reynolds (Re) and Nusselt (Nu) numbers. Wasan and Baid [5] focused on the HWA response in a carbon dioxide-air mixture, by performing a calibration in pure gases, and then used a linear approximation to estimate velocities. All these methods are characterised by a considerable uncertainty, especially when the two components have molecular weights significantly different one to the other [7]. McQuaid and Wright [10] examined the response of HWA in gas mixtures, defining an empirical relation between the molal concentration of the second component gas mixture and the voltage response. The main result of this study was the empirical correction on the response of HWA in presence of gases other than air. A different approach was proposed by Talbot et al. [11]. They performed neon-doping in a variable-viscosity flows of propane-air mixture, and showed the hot-wire response to be insensitive to the concentration field. Zhu et al. [12] analysed velocity and turbulence within the dense gas plumes by using hot-film anemometry with an optimum overheat ratio that allowed them to perform measurements in a range of carbon dioxide (CO_2) concentration (less than 25%) that did not affect the probe sensitivity. Over the range of 0.3-1.1 m/s, the errors in the mean wind speeds were generally less than 5%. Finally, Banerjee and Andrews [7] performed a detailed procedure to investigate helium-air mixture with HWA, employing a multiposition-multioverheat hot-wire technique to estimate both velocity and density fluctuations and defining a calibration surface in function of density and velocity.

Coupled measurements of velocity and concentration were most commonly performed with a HWA-FID or HWA-PID system, with the exceptions of Raupach and Legg [13] and Stapountzis et al. [14], who employed the HWA and a cold wire to measure the velocity and scalar field, respectively (since they simulated the scalar source with a heated wire). Fackrell and Robins [15] measured with HWA-FID the first two moments of the concentration field of a passive scalar plume and estimated the turbulent mass fluxes induced by a point source of varying size and height in a turbulent boundary layer. Koeltzsch [16] used the same technique to estimate the turbulent mass

fluxes in a similar set-up, focusing on the dependence of the turbulent Schmidt number on the distance from the wall. Metzger and Klewicki [17] developed a sensor combining HWA with a PID. Talluru et al. [18] used this same system to investigate passive scalar dispersion in a turbulent boundary layer.

Others studies used a coupled system of LDA-FID to directly estimate turbulent fluxes of a passive scalar [19, 20, 21]. Employing the LDA [22] for the velocity measurements prevents any calibration uncertainty related to a varying density difference, but may imply other complications. Notably, the aerosols used to seed the flow may affect the concentration statistics measured by the FID. To analyse these and other metrological aspects of these coupled measurements techniques, Marro et al. [23] compared the HWA-FID and the LDA-FID systems, notably concerning the optimal distance between the probes (which was found to be equal to 4 mm, i.e. $0.2L$, being L the Eulerian integral length scale), the evaluation of the time lag (16 ms) of the measured signals of concentration and velocity, the effect of the seeding on the concentration statistics for the LDA-FID coupled system. After having defined the optimal settings of the probes, they enlightened the reliability of both systems for simultaneous measuring of high-frequency signals of velocity and concentration in a turbulent boundary layer. This study showed also that the computations of the cross-correlations between velocity and scalar fields with two different methods - slot correlation technique [24, 25] and sample-and-hold reconstruction and resampling - were in good agreement [23].

It is worth noting that these coupled techniques have not been used so far to investigate the dispersion of heavy gas releases. To that purpose, the release of a heavy gas can be conveniently produced by a mixture of air and carbon dioxide [26, 27, 28, 29, 30, 31]. The local density within the turbulent flow can then be evaluated by a direct estimate of the heavy gas concentration [26, 32] or, alternatively, by adding a tiny quantity of a gas tracer, whose presence can be detected with a FID. Common tracers are propane [33] and ethane (C_2H_6) [27, 12, 31]. Schatzmann et al. [27] and Donat and Schatzmann [34] used a gas-probe sampling system connected to a FID to analyse time averaged concentrations and velocities of heavy gas plumes. Robins et al. [33] collected simultaneously 16 air samples using a vacuum system and analysed it with a FID, to estimate the mean concentration field in neutral turbulent boundary layer. They

used two additional channels for the calibration, one to determine the background hydrocarbon concentration in the wind tunnel and the other to obtain the sensor response of the calibration gas of known and certified composition. Britter and Snyder [31] measured with a FID the time averaged concentration field induced by a steady emission of a passive scalar and a heavy gas. They calibrated the FID using an ethane-air mixture and investigated separately the response of the FID to ethane-air-carbon dioxide mixture, and corrected the measurements accordingly. Zhu et al. [12] investigated a ground-level emission of heavy gas, using ethane as tracer and CO_2 as heavy gas, imposing a ratio between carbon dioxide and ethane $r = C_{CO_2}/C_{C_2H_6} = 33.3$. Moreover, they tested the response of the FID to ethane-air and ethane-air-carbon dioxide mixtures in a series of measurements, in which the source mixtures were diluted with air at constant rates in a dilution chamber. The same method was employed by Snyder [28]. Recently, Robins et al. [35] performed wind-tunnel experiments of non-buoyant and dense gas dispersion in complex geometries providing a data set for the mean concentration in the framework of the MODITIC project.

This work is part of a project that aims at studying heavy gas dispersion from an elevated-point source in a turbulent atmospheric boundary layer. Following the recent works of Iacobello et al. [36] and Marro et al. [23] on passive scalar emissions, we use a coupled system of HWA-FID to investigate the release of a dense mixture of air, CO_2, and ethane. The aim of the present study is to define a calibration procedure for both the FID and the HWA that takes into account the influence of the mixture density on the measuring instruments. In this new approach, the instantaneous measurements of concentration are used to provide a time-dependent correction of the HWA response. In this way, we could extend former studies on turbulent dispersion of passive scalars to the case of negatively buoyant releases. This method allows high-frequency simultaneous measurements of velocity and concentration to be performed within heavy gas plume and, therefore, it opens new perspectives for the investigation of the dynamics of dense gas dispersion in the atmosphere.

In what follow, we first present the experimental setup used for the calibration and the wind-tunnel experiments (Section 2.1). We continue by describing the characteristics of the instruments (Section 2.2 and 2.3) and the coupled measurement system

(Section 2.4). The calibration procedures are detailed for the FID (Section 3) and the HWA (Section 4). Finally, we present results on the concentration mean field and the mean, turbulent, and total mass fluxes estimated over cross-wind sections, verifying the conservation of the mass within the plume and, therefore, the reliability of the coupled measurement technique (Section 5).

2. Experimental methods

2.1. Experimental setup

The experiments are conducted in the atmospheric wind tunnel of the Laboratoire de Mécanique des Fluides et d'Acoustique (LMFA) at the École Centrale de Lyon in France. The recirculating wind tunnel is 14 m long, 3.7 m wide, and 2 m high with an adjustable ceiling to control pressure gradients. The temperature in the test section is regulated to limit the temperature variation during a one-day experiment in the range ± 0.5°C. The wind-tunnel temperature - in a range between 21°C and 26°C - is chosen to minimise the temperature difference between the emitted gases (coming from pressurised bottles) and the wind-tunnel flow.

In order to calibrate the instruments, a mixture of air, ethane, and carbon dioxide is used to generate density controlled gas mixtures. Ethane is employed as a tracer as the FID is sensitive to its concentration [37]. Ethane has almost the same density of air (ρ_a), while the density of CO_2 is about $1.5\,\rho_a$. Different fractions of carbon dioxide are used to modify the density of the gas mixture during the calibration and the experiments. The mixture device is composed by three different lines (Figure 1), one for each gas. Every line is equipped with a digital mass-flow controller (Alicat Scientific MC-Series) that integrates a proportional–integral–derivative controller and provides the volumetric flow rate Q_v for each gas. The mass-flow controllers work in a range between 1 and 20 Nl/min for CO_2 and air, and between 0.50 and 200 Nml/min for ethane. The error on the mass-flow rate is estimated by comparison with measurements provided by a volumetric counter. The maximal difference between the measurements of the two instruments does not exceed $\pm 3\%$ [38]. Between the CO_2 tank and the flow-meter is placed a heater, to avoid the presence of condensed CO_2 droplets that could

change the dynamics of the dispersion and the response of the instruments. All the lines are connected to a valve in which gases are blended together before being directed to the source, as shown in Figure 1. The concentrations of ethane and CO_2 at the source are computed in volumetric ppm, and referred to as $c_s = Q_v/Q_{v,s}$, where Q_v is the flow rate of the considered gas and $Q_{v,s}$ the total flow rate at the source, expressed in l/min.

The steady releases of a heavy gas and a passive scalar are investigated in a neutral turbulent boundary layer characterised by free-stream velocity $U_\infty = 1.45$ m/s and height $\delta = 0.8$ m. The turbulent boundary layer is generated by combining the effects of spires and wall roughness, as described in Nironi et al. [38]. The plume is released from a metallic stack of internal diameter $d_s = 0.012$ m and placed at $h_s = 0.076$ m from ground level and at 7.5δ from the beginning of the working section, where the boundary layer can be considered fully developed (Figure 1). The heavy gas release is a mixture of air, ethane, and CO_2, whereas the passive scalar plume consists of an air-ethane mixture. The sampling duration is $300\,s$, allowing the stochastic uncertainty of the concentration statistics (due to the finite size of the sampling) to be of order 0.1 % [38]. The flow rate at the source is $Q_{v,s} = 16.0$ Nl/min for both heavy and passive releases, corresponding to a vertical velocity of $w_s = 2.37$ m/s. For the heavy gas emission the volume flow of CO_2 is 14.8 Nl/min, which corresponds to a density at the source $\rho_s \approx 1.78$ kg/m^3 (depending on the temperature in the wind tunnel) and to a relative density difference $\Delta\rho_s/\rho_a = (\rho_s - \rho_a)/\rho_a \approx 50\%$.

2.2. Concentration measurements

Concentration is measured with the FID Cambustion HFR400 system, consisting of a module for hydrocarbon sampling and an electronic control unit [39], that is sensitive to the presence of hydrocarbons [37]. The gas sample is sucked and burned in the combustion chamber where a cathode collects ions. The instrument returns the electric potential difference induced by the ionization current, proportional to the number of atoms of carbon in the gas tracer sampling. The complex combustion process produces a series of chemical reactions that occur in the combustion chamber. The presence in the sample of gases other than the tracer, such as CO_2, influences these reactions, changing the instrument response. We fix the ratio $r = C_{CO_2}/C_{C_2H_6}$ between

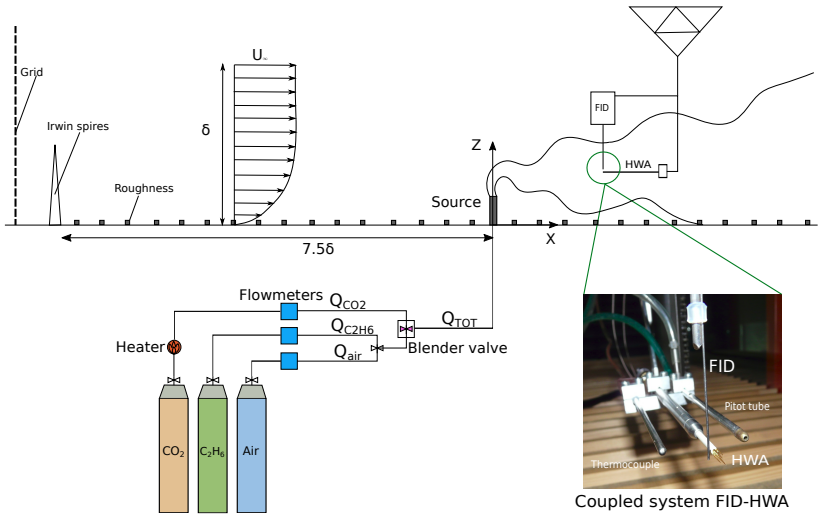

Figure 1: Experimental setup of gas lines and coupled measurements system

carbon dioxide and ethane concentration at the source and we assume that r is constant all along the dispersion process. This is justified by the fact that molecular diffusion coefficient in air for CO_2 and ethane are comparable $D_{CO_2} = 1.61 \times 10^{-4}$ m^2/s and $D_{C_2H_6} = 1.48 \times 10^{-4}$ m^2/s at 20 °C [40] and that the gases are well blended at the emission. The FID is equipped with a sampling tube 0.3 m long and a diameter of 0.125 mm. Its frequency response is approximately 400 Hz [23].

Since the experiments are performed in a recirculating wind tunnel, the increase of background concentration over time has to be taken into account. We therefore measure the background concentration before and after the registration of each concentration time series, we perform a linear interpolation and, finally, we subtract the interpolated values from the signal.

2.3. Velocity measurements

Velocity measurements are performed with X-wire probe HWA at constant temperature [41, 42], of Dantec Dynamics (Streamline 90N10 Frame, with CTA Module 90C10). The platinum probe wire is 1 mm long and with a diameter of 5 μm and is connected to one arm of a Wheatstone bridge. Its velocity-vector acceptance angle is 45°. In our setup, the HWA has a frequency response of about 5000 Hz. The yaw

calibration is not performed. After the calibration procedure, described in Section 4, we apply a yaw correction with constant coefficients $k_1^2 = k_2^2 = 0.0225$ to decompose velocities from the X-probe into longitudinal and transverse velocity components [43]. Since the HWA response is influenced by the CO_2 concentration, it is necessary to know the instantaneous value of this concentration in the sampling volume to correct the HWA response. This is made possible through the coupled HWA-FID measurement system.

2.4. Coupled measurement system HWA-FID

A coupled HWA-FID system requires the setting of an optimal distance between the two probes so that these are: i) sufficiently far to avoid any perturbation on the response of one instrument on the other, and ii) sufficiently close to consider measurements as performed in the same sampling volume [23]. According to the analysis presented in Marro et al. [23] this distance is set to 5 mm.

In proximity of the coupled HWA-FID system, we install a Pitot-static tube and a thermocouple monitoring, respectively, the flow velocity and the air temperature during the experiment. The Pitot-static tube provides a verification of the (time averaged) longitudinal velocity provided by the HWA measurements, whereas the thermocouple allows us to check that the temperature inside the wind tunnel is constant ($\pm 0.5^{\circ}$C) during the sampling. This is an important requirement to perform HWA measurements without the need of re-calibrating the instrument [43].

The sampling frequency for coupled measurements (HWA and FID) is set at 1000 Hz. Signals of concentration are shifted in time by 16 ms with respect to velocity, which is the time required for the gas sample to reach the FID combustion chamber [23]. Once time shifted, the signals do not need resampling and we can compute the cross statistics.

According to the measurements of Nironi et al. [38], the experimental error, estimated by repeating the measurements in a fixed reference location, is 2% for the mean and the standard deviation of the velocity, and 3% for the mean and the standard deviation of the concentration. With a similar experimental setup, Marro et al. [23] assessed similar values for the LDA-FID system. Both studies were however performed with

passive scalar releases.

3. FID calibration in the presence of CO_2

The calibration is performed by connecting the output of a three lines mixture device to a pipe of diameter 0.005 m, with a temperature in the test section in the range 21-26°C. The FID is placed at the exit of this pipe and we investigated the response of the probe for different mixtures of CO_2 and ethane. Figure 2a shows the response of FID, in volt $E(V)$, as a function of the ethane concentration, for different ratio $r = C_{CO_2}/C_{C_2H_6}$ of the gas mixture. We note that $E(V)$ decreases as the ratio r increases. This means that, for a constant $C_{C_2H_6}$, the presence of C_{CO_2} reduces the voltage response. Secondly, for pure ethane or low value of r, it is possible to define the ethane concentration as a one-to-one function of volts provided by the FID ($r = 36$ in Figure 2a). As C_{CO_2} increases ($r \geq 75$), a saturation of the signal occurs and the relation between $E(V)$ and $C_{C_2H_6}$ is no longer one-to-one. The calibration curves collapse on a single curve when the products between $E(V)$ and the ratio r are plotted versus the density of the mixture ρ (Figure 2b). This analysis allows us to identify a unique critical density $\rho_c = 1.56$ kg/m^3 in the whole range of values of r (red line in Figure 2b), corresponding to 58% of CO_2. Measurements performed in a mixture with density $\rho < \rho_c$ are, therefore, calibrated with a one-to-one function. Since we impose a constant plume density $\rho_s > \rho_c$ at the stack, we cannot perform measurements very close to the source due to the saturation of FID and, therefore, we have to carefully choose the minimal sampling distance from the release point. We could check that at $X = 0.250\delta$ the dispersion process ensured that the condition $\rho < \rho_c$ was fulfilled.

To avoid FID saturation, we impose $50 < r < 60$ for measurements close to the source, and $12 < r < 30$ for measurements in the far field. As a general rule, FID calibration is performed twice a day during the whole experimental campaign.

4. HWA Calibration in CO_2-air mixtures

When performing the HWA calibration, the standard procedure determines the sensitivity coefficients of the two wires with respect to different flow variables [3]. This

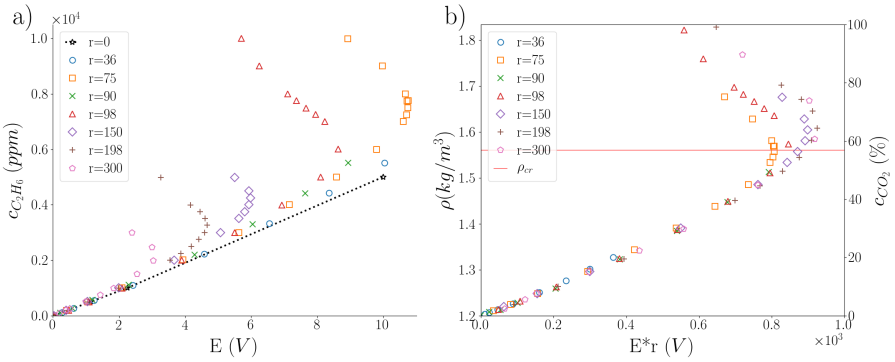

Figure 2: FID calibration curves for varying $r = C_{CO_2}/C_{C_2H_6}$. a) Ethane concentration as a function of volt response E (the dotted line refers to the case of pure ethane). b) Normalized gas-mixture density as a function of rE.

relation depends on velocity, ambient temperature, and gas-mixture density. Here, we are particularly concerned with the effect of a varying density on the HWA response. In this study, we use a similar approach to that used by Banerjee and Andrews [7] for the HWA calibration in the context of a heavy gas atmospheric dispersion. The main conceptual difference between our work and the one of Banerjee and Andrews [7] is that we use this calibration to perform simultaneous and distinct measurements of concentration and velocity. As already stated, the temperature in the test section of the wind tunnel is kept constant during one experiment, but the HWA calibration needs to be repeated every time the temperature varies more than ± 0.5°C. The calibration of the hot-wire anemometer is performed at the exhaust of a pipe of 25 mm in diameter and 700 mm long. We use a gas mixture of CO_2 and air with five different ratios of the mixture, between 0 and 100%. The procedure includes a velocity correction using Pitot-static tube measurements, to take into account the difference between the velocity at the centre of the profile of the turbulent flow in the pipe and the average velocity over the tube section, as estimated by the flow-meters. From the measurements with the Pitot-static tube, we identify a 3rd degree polynomial linking the flow rate and the velocity in the range 0 to 3 m/s, that is the velocity range in the experiments. The velocity U is reported in Figure 3a as a function of the volt response E_1, each set corresponding to a different percentage of carbon dioxide. These data can be fitted by a

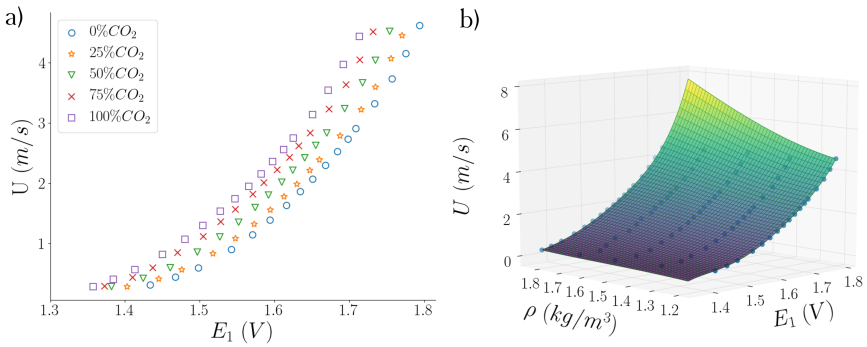

Figure 3: a) HWA calibration curves for gas mixture with increasing quantities of CO_2: velocities vs volt response. b) HWA calibration surface velocities vs volt response and gas-mixture density.

bi-dimensional function that takes into account the dependence of the velocity on both $E_1(V)$ and ρ (Figure 3b). The surface is a polynomial fit of 5th (for E_1) and 4th (for ρ) degree of the form $U(\rho, E_1) = \sum_{i=0}^{5} \sum_{j=0}^{4} p_{ij} E_1^i \rho^j$, where the coefficients p_{ij} are set for each calibration. The maximal discrepancies between the fit surface and the actual measurements is equal to 2.7% and occurs for small velocities (notably for $U = 0.58$ m/s), namely due to the uncertainties related to the flow-meters. In order to use the calibration surface $U(\rho, E_1)$ for instantaneous velocity measurements, the coupled system is essential. The estimates of the instantaneous concentrations provided by the FID allow us to evaluate the instantaneous density of the fluid and thus convert accordingly the HWA volt response.

5. Measurements and analysis

We investigate the steady release of a heavy gas and a passive scalar in a neutral turbulent boundary layer (Section 2.1), performing simultaneous measurements of concentration and velocity profiles downwind the source with the coupled system HWA-FID. For each measurement section we measure two profiles: a vertical profile on the plume axis (y=0) and a transverse profile at a varying vertical height, corresponding to that of the maximum value of the mean concentration, as identified in the vertical profile.

To compare the results we employ dimensionless concentration and velocities. The latter are denoted as u^*, w^*, v^* and are re-scaled by the free-stream velocity U_∞. The non-dimensional concentration c^* is instead normalised as:

$$c^* = c\,\frac{U_\infty \delta^2}{Q_s} \tag{1}$$

In Figure 4 is reported the normalised time averaged concentration, referred to as $\overline{c^*}$, for a heavy gas plume and a passive scalar, i.e. neutral density emission. Each profile corresponds to a section at increasing distances from the source. We observe that, as $\overline{c^*}$ decreases downstream the source, the heavy gas plume develops close to the ground and it is deflected, due to the negative buoyancy effects. We reported in the upper x-axis the relative averaged density difference, defined as $\Delta\overline{\rho}/\rho_a = (\overline{\rho} - \rho_a)/\rho_a$. The larger density differences are of course observed close to the source. The maximal averaged density difference across the first measurement section ($X/\delta = 0.25$) is slightly less than 3%, about 1.5% at the second section, and further reduced away from the source. These averaged values are considerably smaller than the typical range of density differences over which the FID has been calibrated. Note however that the aforementioned averaged values are computed on highly intermittent signals, in which peak instantaneous values can be more than 10 times larger than the mean value. Since the calibration curve is not linear (in presence of CO_2), this latter has to be applied to instantaneous concentrations. These features highlight the need for an accurate calibration procedure to obtain reliable concentration statistics.

Employing our coupled measurement system, adjusted with the HWA and the FID calibration, we can also obtain simultaneous measurements of concentration and velocity, that allow us to measure vertical profiles of streamwise turbulent mass fluxes, referred to as $\overline{u'c'}^*$, reported in Figure 5a in dimensionless values. As for $\overline{c^*}$, the intensity of $\overline{u'c'}^*$ decreases with increasing distance from the source as the plume spreads. The vertical displacement of the plume has also a role on the spatial evolution of $\overline{u'c'}^*$, for the heavy gas emission. Close to the source, the dispersion dynamics is significantly influenced by the emission conditions: the source momentum and buoyancy alter the velocity field, resulting in values of $\overline{u'c'}^*$ at the plume centre that are lower for the heavy gas plume (≈ -7), compared to those observed for the passive scalar release

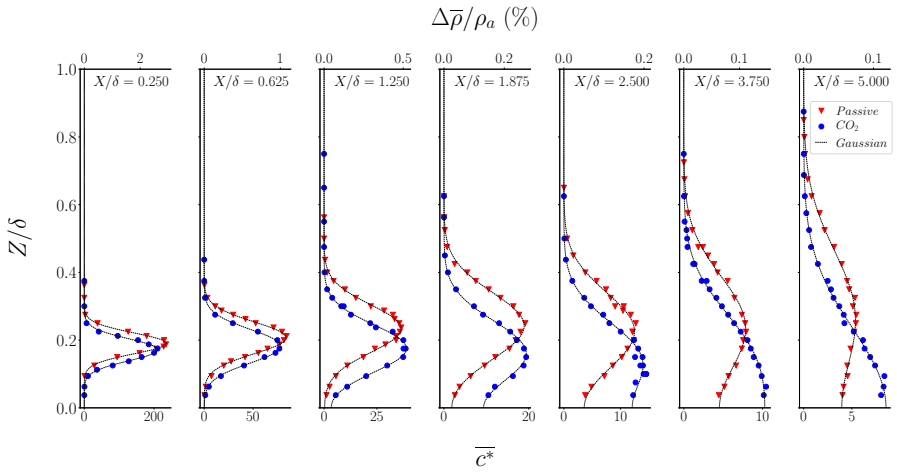

Figure 4: Vertical profiles of the normalized time averaged concentration $\overline{c^*}$ and relative density difference $\Delta\overline{\rho}/\rho_a$ at increasing distance from the source for passive (red) and heavy (blue) gas plumes.

(≈ -5). Moving further away from the source, the peak values of the horizontal turbulent mass fluxes are similar for the passive and heavy gas, and the mass fluxes gradients are progressively smoothed. The profiles present a vertical displacement strictly related to the different trajectory of the plume, as showed in Figure 4.

We estimate the vertical profiles of the longitudinal time-averaged mass fluxes as the product between the mean concentration and mean velocity profiles (Figure 5b). The general trend follows that previously observed for the mean concentration profiles (Figure 4), with the heavy gas plume deflected towards the ground. Furthermore, near the source, the maximum of the streamwise mean mass fluxes is slightly lower for the heavy gas plume compared to the passive one. For increasing distance from the source, the maximum values of $\overline{u^*} \cdot \overline{c^*}$ are higher in case of heavy gas release.

In order to evaluate the reliability of our measurements, we have verified the mass conservation downwind the source, by comparing the integrated mass flux at different cross-flow sections, $Q(x)$, to the mass-flow rate Q_s released at the source location, i.e.:

$$\frac{Q}{Q_s} = \int\int \overline{uc}^* \, dy^* dz^*, \tag{2}$$

where $y^* = y/\delta$ and $z^* = z/\delta$.

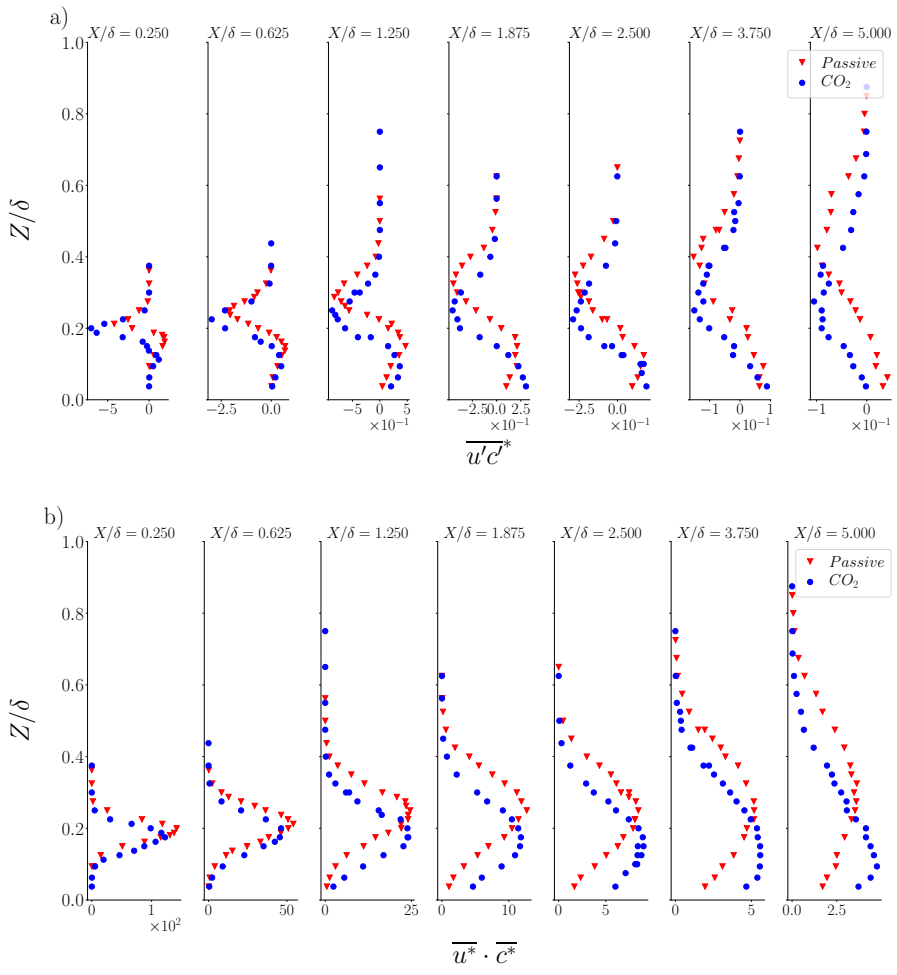

Figure 5: Vertical profiles of a) normalized longitudinal turbulent mass fluxes and b) normalised longitudinal mean mass fluxes for sections at increasing distance from the source for passive and heavy gas plume.

Adopting the Reynolds decomposition, the mass fluxes can be expressed as the sum of the mean and the fluctuating component:

$$\overline{uc}^* = \overline{u^*}(z) \cdot \overline{c^*}(x,y,z) + \overline{u'c'}^*(x,y,z). \tag{3}$$

The available information on $\overline{c^*}(x,y,z)$ and $\overline{u'c'}^*(x,y,z)$ are limited on the vertical and transverse profiles, crossing at the plume centre. To evaluate the mass fluxes on the entire cross-section, some hypotheses have to be made. Concentration profiles are fitted with a Gaussian function for the transverse profiles and a double symmetric Gaussian profile in the vertical direction (to take into account the reflection of the plume to the ground). We assume a velocity profile homogeneous in the horizontal plane, whereas the dependence on the distance from the wall follows a classical power-law (see Nironi et al. [38]). For the turbulent mass fluxes $\overline{u'c'}^*$, we linearly fit the measured vertical profiles and assume a Gaussian for the transverse profiles, since the information collected from the measurements were not sufficient to estimate a more specific shape. Despite the large number of approximations adopted to estimate the total mass flux, we believe that this procedure provides a useful check of the reliability of the experimental results.

In Figure 6 we plot Q/Q_s as a function of the longitudinal distance from the source (Figure 6). Similar comparisons were performed by Raupach and Legg [13] and, more recently, by Marro et al. [23] in the case of passive emissions. Raupach and Legg [13] evaluated the streamwise heat flux induced by an elevated linear source, obtaining values with a range of variation up to 20%, with a clearly decreasing trend for increasing distances from the source. As pointed out by the authors, this decreasing trend was due to the heat losses at the lateral walls of the wind tunnel. Marro et al. [23] analysed instead the case of a chemical tracer emitted from a ground-line source and observed a global uncertainty on Q/Q_s of about 8%, that did not depend on the distance from the source. Since we use here the same measurement techniques (and same instruments) used by Marro et al. [23], we adopt as a reference the same uncertainty for the mass fluxes, and therefore we plot 8% error bars in the estimates presented in Figure 6.

As Figure 6 shows, the total fluxes Q/Q_s for both the passive and the heavy gas release are slightly underestimated. The discrepancies with the reference value $Q/Q_s = 1$

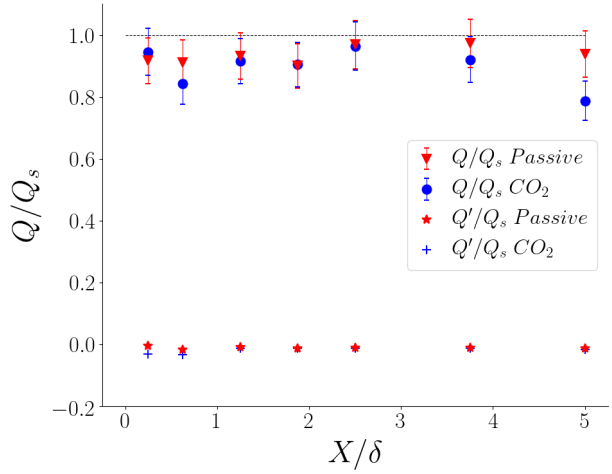

Figure 6: Integrated flux over transverse sections normalized by the flow rate at the source Q_s, for increasing distance from the source.

never exceed 20% and are on average approximately 10%. Of course, these differences between our estimates and the reference value are here larger than those observed by Marro et al. [23]. This is due to the fact that we are here dealing with a 3D plume, whose structure is reconstructed by fitting two profiles only. Instead, the 2D plume examined by Marro et al. [23] could be fully characterised by a single profiles of velocity and concentration statistics (at each downstream location). However, note that the discrepancies between our estimates and the reference value $Q/Q_s = 1$ are very similar for the passive scalar and the heavy gas release. We can therefore assert that our measurements in the heavy gas plume are as reliable as those performed within a passive scalar plume.

In Figure 6 we also report the normalized fluctuation fluxes (Q'/Q_s), which are shown to be negative. Their values are low and they contribute for less than 2% to the total mass flux, a value which is systematically lower than that estimated by Marro et al. [23] for a line ground-level source. This difference can be explained by noting that, when the plume is elevated, $\overline{u'c'}^*$ has opposite signs above and below the plume centreline (as it can be inferred from Figure 5a). Once the plume becomes ground based, $\overline{u'c'}^*$ becomes instead purely negative.

In Figure 7 we compare the non-dimensional mass fluxes in the cross-flow section for heavy gas (Figure 7a, c, e, and g) and passive scalar (Figure 7b, d, f, and h) releases at increasing distance from the source, with contour values that span from 10^{-3} to 10^{2}. The distribution of the mass flux in the different sections confirms what was highlighted in the previous paragraphs: due to the negative buoyancy the trajectory of the plume is deflected more rapidly toward the ground compared to the passive scalar plume.

6. Conclusions

We have defined a procedure to calibrate a coupled system of HWA-FID in order to measure velocity and concentration statistics within heavy gas plumes. This system provides high-frequency simultaneous concentration and velocity values in the same sampling volume. The heavy gas mixture was composed by CO_2, air, and C_2H_6, the latter used as a tracer, since its concentration was detected by the FID. The presence of CO_2 in the mixture alters the voltage response of both instruments. For this reason, we have analysed the FID response as a function of the ratio $r = C_{CO_2}/C_{C_2H_6}$ and of the mixture density, identifying a critical density that corresponds to the 58% of CO_2 in the mixture and thus a value of $\Delta\rho_c/\rho_a = (\rho_c - \rho_a)/\rho_a \approx 30\%$. For a mixture density lower than this value, we could define a one-to-one function to calibrate the FID. The HWA response depends on both the flow velocity and the density of the gas mixture. We have therefore defined a procedure to estimate a calibration surface accounting for the dependence on both quantities.

This method is affected by some shortcomings. Notably, we are limited to heavy gas clouds whose CO_2 peak-concentration does not have to exceed 58%, in order to calibrate the FID with a one-to-one function. Furthermore, we need to carefully fix the ratio between carbon dioxide and gas tracer. In particular, we impose a high r value close to the source to prevent FID saturation, whereas we adopt releases with a lower r in order to perform measurements in the far field, so that the ethane concentration is high enough to be detectable with the FID.

As a demonstration, we employed the coupled system HWA-FID in wind-tunnel experiments, simulating a passive scalar and a heavy gas release from an elevated stack.

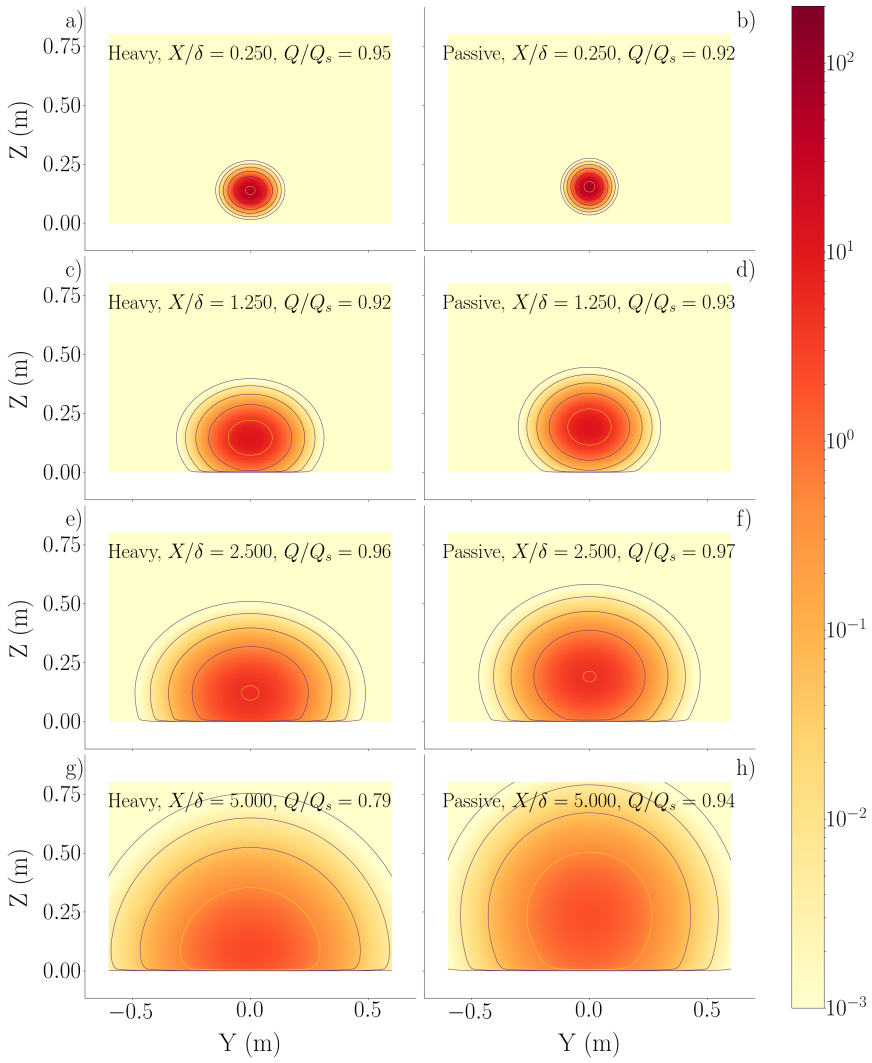

Figure 7: Mass fluxes in the cross-flow section for increasing section from the source for a), c), e), g), heavy gas and b), d), f), h), passive plume.

We measured the pollutant concentration field downwind the source and analysed the dimensionless mean concentration $\overline{c^*}$. This clearly showed the effect of buoyancy on the development of the heavy gas plume downwind the source. Simultaneous measurements of concentration and velocity allowed us to obtain vertical profiles of streamwise turbulent mass fluxes $\overline{u'c'}^*$. The distribution of the mass flux in the cross-flow sections enlightened the vertical displacement of the heavy gas plume, compared to the passive scalar, due to its negative buoyancy. The estimates of the longitudinal mean and turbulent mass fluxes allowed us to evaluate the total mass fluxes as $\overline{uc^*} = \overline{u^*} \cdot \overline{c^*} + \overline{u'c'}^*$. We integrated $\overline{uc^*}$ in the cross-flow section of the plume at increasing distances from the source and we compared these values to the mass-flow rate provided by the flow-meter in order to verify the integral mass balance. We found that the differences were of about 10% for both the passive scalar and the heavy density releases. This shows that the two sets of data have a similar accuracy and, therefore, the calibration process developed in this study provides measurements for a heavy gas plume that are as reliable as those obtained for a passive scalar plume.

Acknowledgements

C. Vidali is funded by Air Liquide.

References

[1] R. E. Britter, Atmospheric dispersion of dense gases, Annual Review of Fluid Mechanics 21 (1989) 317–344.

[2] R. N. Meroney, Guidelines for fluid modeling of dense gas cloud dispersion, Journal of Hazardous Materials 17 (1987) 23 – 46.

[3] G. Comte-Bellot, Hot-wire anemometry, Annual Review of Fluid Mechanics 8 (1976) 209–231.

[4] R. L. Simpson, W. G. Wyatt, The behaviour of hot-film anemometers in gas mixtures, Journal of Physics E: Scientific Instruments 6 (1973) 981–987.

[5] D. T. Wasan, K. M. Baid, Measurement of velocity in gas mixtures: Hot-wire and hot-film anemometry, AIChE Journal 17 (1971) 729–731.

[6] W. M. Pitts, B. J. McCaffrey, Response behaviour of hot wires and films to flows of different gases, Journal of Fluid Mechanics 169 (1986) 465–512.

[7] A. Banerjee, M. J. Andrews, A convection heat transfer correlation for a binary air-helium mixture at low Reynolds number, Journal of Heat Transfer 129 (2007) 1494–1505.

[8] J. Way, P. A. Libby, Hot-wire probes for measuring velocity and concentration in helium-air mixtures, AIAA Journal 8 (1970) 976–978.

[9] S. Corrsin, Extended applications of the hot-wire anemometer, Review of Scientific Instruments 18 (1947) 469–471.

[10] J. McQuaid, W. Wright, The response of a hot-wire anemometer in flows of gas mixtures, International Journal of Heat and Mass Transfer 16 (1973) 819 – 828.

[11] B. Talbot, N. Mazellier, B. Renou, L. Danaila, M. A. Boukhalfa, Time-resolved velocity and concentration measurements in variable-viscosity turbulent jet flow, Experiments in Fluids 47 (2009) 769.

[12] G. Zhu, S. Arya, W. H. Snyder, An experimental study of the flow structure within a dense gas plume, Journal of Hazardous Materials 62 (1998) 161 – 186.

[13] M. R. Raupach, B. J. Legg, Turbulent dispersion from an elevated line source: measurements of wind-concentration moments and budgets, Journal of Fluid Mechanics 136 (1983) 111–137.

[14] H. Stapountzis, B. L. Sawford, J. C. R. Hunt, R. E. Britter, Structure of the temperature field downwind of a line source in grid turbulence, Journal of Fluid Mechanics 165 (1986) 401–424.

[15] J. E. Fackrell, A. G. Robins, Concentration fluctuations and fluxes in plumes from point sources in a turbulent boundary layer, Journal of Fluid Mechanics 117 (1982) 1–26.

[16] K. Koeltzsch, The height dependence of the turbulent Schmidt number within the boundary layer, Atmospheric Environment 34 (2000) 1147 – 1151.

[17] M. M. Metzger, J. C. Klewicki, Development and characterization of a probe to measure scalar transport, Measurement Science and Technology 14 (2003) 1437–1448.

[18] K. M. Talluru, C. Hernandez-Silva, J. Philip, K. A. Chauhan, Measurements of scalar released from point sources in a turbulent boundary layer, Measurement Science and Technology 28 (2017) 055801.

[19] D. Contini, P. Hayden, A. Robins, Concentration field and turbulent fluxes during the mixing of two buoyant plumes, Atmospheric Environment 40 (2006) 7842 – 7857.

[20] M. Carpentieri, A. G. Robins, Tracer flux balance at an urban canyon intersection, Boundary-Layer Meteorology 135 (2010) 229–242.

[21] M. Carpentieri, P. Hayden, A. G. Robins, Wind tunnel measurements of pollutant turbulent fluxes in urban intersections, Atmospheric Environment 46 (2012) 669 – 674.

[22] J. Abbiss, T. Chubb, E. Pike, Laser Doppler anemometry, Optics & Laser Technology 6 (1974) 249 – 261.

[23] M. Marro, H. Gamel, P. Méjean, H. Correia, L. Soulhac, P. Salizzoni, High-frequency simultaneous measurements of velocity and concentration within turbulent flows in wind-tunnel experiments, Experiments in Fluids 61 (2020) 245.

[24] E. Müller, H. Nobach, C. Tropea, A refined reconstruction-based correlation estimator for two-channel, non-coincidence laser Doppler anemometry, Meas. Sci. Technol. 9 (1998) 442–451.

[25] H. Nobach, Present methods to estimate the cross-correlation and cross-spectral density for two-channel laser Doppler anemometry, in: 18th International Symposium on the Application of Laser and Imaging Techniques to Fluid Mechanics, Lisbon, Portugal, 4–7 July, 2016.

[26] R. N. Meroney, Wind-tunnel experiments on dense gas dispersion, Journal of Hazardous Materials 6 (1982) 85 – 106.

[27] M. Schatzmann, W. H. Snyder, R. E. Lawson, Experiments with heavy gas jets in laminar and turbulent cross-flows, Atmospheric Environment. Part A. General Topics 27 (1993) 1105 – 1116.

[28] W. H. Snyder, Wind-tunnel study of entrainment in two-dimensional dense-gas plumes at the EPA's fluid modeling facility, Atmospheric Environment 35 (2001) 2285 – 2304.

[29] G. Briggs, R. Britter, S. Hanna, J. Havens, A. Robins, W. Snyder, Dense gas vertical diffusion over rough surfaces and results of wind-tunnel studies, Atmospheric Environment 35 (2001) 2265–2284.

[30] S. R. Hanna, J. C. Chang, Use of the Kit Fox field data to analyze dense gas dispersion modeling issues, Atmospheric Environment 35 (2001) 2231 – 2242.

[31] R. E. Britter, W. H. Snyder, Fluid modeling of dense gas dispersion over a ramp, Journal of Hazardous Materials 18 (1988) 37 – 67.

[32] G. Briggs, R. E. Britter, S. R. Hanna, J. Havens, S. B. King, A. G. Robins, W. H. Snyder, K. W. Steinberg, Advances in Dense Gas Dispersion Modeling of Accidental Releases over Rough Surfaces during Stable Conditions, Springer US, Boston, MA, 1998, pp. 509–516.

[33] A. Robins, I. Castro, P. Hayden, N. Steggel, D. Contini, D. Heist, A wind tunnel study of dense gas dispersion in a neutral boundary layer over a rough surface, Atmospheric Environment 35 (2001) 2243 – 2252.

[34] J. Donat, M. Schatzmann, Wind tunnel experiments of single-phase heavy gas jets released under various angles into turbulent cross flows, Journal of Wind Engineering and Industrial Aerodynamics 83 (1999) 361–370.

[35] A. Robins, M. Carpentieri, P. Hayden, J. Batten, J. Benson, A. Nunn, MODITIC wind tunnel experiments, in: 17th International Conference on Harmonisation

within Atmospheric Dispersion Modelling for Regulatory Purposes, Budapest, Hungary, 9-12 May, 2016.

[36] G. Iacobello, M. Marro, L. Ridolfi, P. Salizzoni, S. Scarsoglio, Experimental investigation of vertical turbulent transport of a passive scalar in a boundary layer: Statistics and visibility graph analysis, Phys. Rev. Fluids 4 (2019) 104501.

[37] J. E. Fackrell, A flame ionisation detector for measuring fluctuating concentration, Journal of Physics E: Scientific Instruments 13 (1980) 888.

[38] C. Nironi, P. Salizzoni, M. Marro, P. Mejean, N. Grosjean, L. Soulhac, Dispersion of a passive scalar fluctuating plume in a turbulent boundary layer. Part I: Velocity and concentration measurements, Boundary-Layer Meteorology 156 (2015) 415–446.

[39] C. Ltd., HFR400 - Fast Response Hydrocarbon Measurement System - User Manual, Technical Report, Cambustion Limited, 2006.

[40] D. T. Pritchard, J. A. Currie, Diffusion of coefficients of carbon dioxide, nitrous oxide, ethylene and ethane in air and their measurement, Journal of Soil Science 33 (1982) 175–184.

[41] A. E. Perry, G. L. Morrison, A study of the constant-temperature hot-wire anemometer, Journal of Fluid Mechanics 47 (1971) 577–599.

[42] H. H. Bruun, Hot-wire anemometry: Principles and signal analysis, Measurement Science and Technology 7 (1996).

[43] F. E. Jorgensen, How to measure turbulence with hot-wire anemometers - a practical guide, Technical Report, Dantec Dynamics, 2002.